November 2017

Initial Mass Function Variability (or Not) among Low-velocity Dispersion, Compact Stellar Systems

Alexa Villaume
University of California, Santa Cruz

Jean Brodie
University of California, Santa Cruz

Charlie Conroy
Harvard-Smithsonian Center for Astrophysics

Aaron Romanowsky
San Jose State University, aaron.romanowsky@sjsu.edu

Pieter van Dokkum
Yale University

Recommended Citation

Alexa Villaume, Jean Brodie, Charlie Conroy, Aaron Romanowsky, and Pieter van Dokkum. "Initial Mass Function Variability (or Not) among Low-velocity Dispersion, Compact Stellar Systems" *The Astrophysical Journal Letters* (2017). https://doi.org/10.3847/2041-8213/aa970f

The Astrophysical Journal Letters, 850:L14 (6pp), 2017 November 20 https://doi.org/10.3847/2041-8213/aa970f

Initial Mass Function Variability (or Not) among Low-velocity Dispersion, Compact Stellar Systems

Alexa Villaume[1], Jean Brodie[1], Charlie Conroy[2], Aaron J. Romanowsky[1,3], and Pieter van Dokkum[4]
[1] Department of Astronomy & Astrophysics, University of California Santa Cruz, 1156 High Street, Santa Cruz, CA 95060, USA
[2] Harvard-Smithsonian Center for Astrophysics, Cambridge, MA 02138, USA
[3] Department of Physics & Astronomy, San José State University, One Washington Square, San Jose, CA 95192, USA
[4] Yale University Astronomy Department, New Haven, CT 06511, USA
Received 2017 September 5; revised 2017 October 26; accepted 2017 October 28; published 2017 November 16

Abstract

Analyses of strong gravitational lenses, galaxy-scale kinematics, and absorption-line stellar population synthesis (SPS) have all concluded that the stellar initial mass function (IMF) varies within the massive early-type galaxy (ETG) population. However, the physical mechanism that drives variation in the IMF is an outstanding question. Here we use new SPS models to consider a diverse set of compact, low-velocity dispersion stellar systems: globular clusters (GCs), an ultra-compact dwarf (UCD), and the compact elliptical (cE) galaxy M32. We compare our results to massive ETGs and available dynamical measurements. We find that the GCs have stellar mass-to-light ratios (*M/L*) that are either consistent with a Kroupa IMF or are slightly bottom-light, while the UCD and cE have mildly elevated *M/L*. The separation in derived IMFs for systems with similar metallicities and abundance patterns indicates that our SPS models can distinguish abundance and IMF effects. Variation among the sample in this paper is only $\sim$50% in normalized *M/L* compared to the $\sim$4$\times$ among the ETG sample. This suggests that metallicity is not the sole driver of IMF variability and additional parameters need to be considered.

Key words: galaxies: star formation – galaxies: stellar content – galaxies: star clusters: general

1. Introduction

The assumption of a universal stellar initial mass function (IMF) has been a cornerstone of stellar population and galaxy evolution studies for decades. Nevertheless, there has been much observational effort to test and challenge this assumption. The work done in nearby systems where it is possible to measure resolved star counts is extensive (see Ch. 9 in Kroupa et al. 2013, and references therein). Since the discovery of surface-gravity-sensitive absorption features (e.g., Wing & Ford 1969), the measurement of the IMF in systems beyond the reach of resolved star counts has been possible. In principle, these lines can measure the ratio of giant-to-dwarf stars in integrated light, which can be used as an IMF proxy (e.g., Cohen 1978; Faber & French 1980; Kroupa & Gilmore 1994).

In practice, only in recent years have the stellar population synthesis (SPS) model precision and near-infrared (near-IR) data quality reached the point where it is possible to measure the dwarf-to-giant ratio. Cenarro et al. (2003) found that age and metallicity effects alone could not explain the variations in CaT strength in a sample of early-type galaxies (ETGs), and tentatively attributed it to IMF variability. More recent work (e.g., van Dokkum & Conroy 2010; Spiniello et al. 2011; Conroy & van Dokkum 2012; Ferreras et al. 2013; Martín-Navarro et al. 2015) has made progress on generating quantitative statements about the relative number of giant and dwarfs stars. The results from SPS modeling broadly agree with investigations using gravitational lensing and kinematics (e.g., Treu et al. 2010; Cappellari et al. 2013). There has been discussion about inconsistencies from different methods on an object-by-object basis (Smith 2014), but the issue was resolved by Lyubenova et al. (2016).

There is not yet a clear physical mechanism driving IMF variability. Metallicity has become a possibility from recent observational work (Martín-Navarro et al. 2015; van Dokkum et al. 2017), but velocity dispersion (σ) and α-element abundances also correlate with IMF variation (Conroy & van Dokkum 2012; La Barbera et al. 2013). Furthermore, there are still unexplained complications in the emerging picture of IMF variability. Newman et al. (2016) demonstrated that even high-velocity dispersion ETGs can have Kroupa (2001; MW) IMFs, and, furthermore, it is not yet clear how IMF variability conforms to the expectations from chemical evolution and star formation measurements (e.g., Martín-Navarro 2016).

Most integrated light probes of the IMF focused on ETGs and so have only looked at IMF variations in relatively narrow regions of parameter space. To better constrain IMF variations as a function of the physical characteristics of the stellar population, we need to push IMF studies to the extremes of parameter space. Ultracompact dwarfs (UCDs) are extremely dense objects that can have high dynamical mass-to-light ratio (*M/L*) values $(M/L)_{dyn}$ (e.g., Mieske et al. 2013). Globular clusters (GCs) are conventionally thought to have MW IMF. However, Strader et al. (2011) found a trend of decreasing $(M/L)_{dyn}$ of M31 GCs as a function of metallicity, in disagreement with the expectation from an MW IMF.

Whether UCDs and GCs actually have variable IMFs and, if so, what the shape may be, is still being debated (Jerabkova et al. 2017). Dabringhausen et al. (2012) took an over-abundance of X-ray binaries in a sample of Fornax UCDs as evidence that those UCDs produced more massive stars than expected from a Kroupa IMF. Marks et al. (2012) used the gas-expulsion timescale of a sample of UCDs and GCs to predict that the IMF would create more massive stars with increasing density. However, Pandya et al. (2016) analyzed 336 spectroscopically confirmed UCDs across 13 host systems and found an X-ray detection fraction of only $\sim$3%. Zonoozi et al. (2016) showed that the combination of a variable IMF and the removal of stellar remnants could plausibly explain the $(M/L)_{dyn}$ trend in the M31 GCs.

Fitting the integrated light of UCDs and GCs with SPS models is needed in order to obtain a more direct measurement of the IMF shape. One caveat is that GCs can be strongly influenced by dynamical evolution, i.e., mass-segregation and evaporation of low-mass stars. For the low-mass stars the "initial" mass function is not being measured, but rather the "present-day" mass function (PDF). However, this should not be a concern for high mass GCs or UCDs; the PDF is expected to closely resemble the IMF owing to long relaxation times (see Equation (17) in Portegies et al. 2010).

In this Letter we present a pilot study of stellar *M/L*s, $(M/L)_*$, of various compact stellar systems (CSSs): M59-UCD3 (Sandoval et al. 2015), three M31 GCs that span a large range of metallicity, and the compact elliptical (cE) M32. For the first time, we fit the spectra of the individual objects with flexible SPS models that allow IMF variability.

2. Observations and Data

All of the objects presented in this Letter were observed with the Low Resolution Imaging Spectrometer (LRIS; Oke et al. 1995), a dual-arm spectrograph on the Keck I telescope on Mauna Kea, Hawaii.

The data for one metal-poor (MP) GC (M31-B058), two metal-rich (MR) GCs (M31-B163 and M31-B193), and M59-UCD3 were obtained on 2014 December 19–20 using the instrument setup and using the same "special" long slit discussed in van Dokkum et al. (2017; $0.7'' \times 290''$). As the objects in this Letter are bright and compact we obtained four 300s exposures using an ABAB pattern where we dithered up and down the slit by $20''$.

Three exposures of 180 s were taken for M32 on 2012 January. The 600 l mm^{-1} grating was used on the blue arm but the same grism as the other objects was used on the red arm. We extracted a spectrum using a square aperture of $0.''8 \times 0.''8$ ($\approx$3 pc).

The intrinsic resolution of the objects in this sample is higher than the models (which are smoothed to a common resolution of $\sigma = 100$ km s^{-1}) so we broadened the spectra in our sample. In order to have roughly the same dispersion in the red for all of the objects, we broadened the M32 and UCD spectra by 150 km s^{-1} and the GCs by 200 km s^{-1}.

3. Modeling

3.1. Model Overview

The methodology we use for fitting the models to data and the parameters fitted are described in detail in Conroy et al. (2017b). The models described in Conroy et al. (2017b; "C2V" models) are the updated versions of the stellar population models from Conroy & van Dokkum (2012; "CvD" models). The most important update for this Letter is the increased metallicity range provided by the Extended IRTF library (Villaume et al. 2017) and metallicity-dependent response functions.

We explore the parameter space using a Fortran implementation of emcee (Foreman-Mackey et al. 2013), which uses the affine-invariant ensemble sampler algorithm (Goodman & Weare 2010). We use 512 walkers, 25,000 burn-in steps, and a production run of 1,000 steps for the final posterior distributions.

We perform full-spectrum fitting. We continuum-normalize the models by multiplying them by higher-order polynomials in order to match the continuum shape of the data.

We sample the posteriors of the following parameters: redshift and velocity dispersion, overall metallicity, a two-component star formation history (two bursts with free ages and relative mass contribution), 18 individual elements, the strengths of five emission line groups, fraction of light at 1 μm contributed by a hot star component, two higher-order terms of the line-of-sight velocity distribution, and nuisance parameters for the data (normalization of the atmospheric transmission function, error, and sky inflating terms).[5]

Additionally, we fit for the slopes of a two-component power-law (break point at 0.5 $M_\odot$):

$$\xi(m) = dN/dm_* = \begin{cases} k_1 m^{-\alpha_1} \text{ for } 0.08 < m < 0.5, \\ k_2 m^{-\alpha_2} \text{ for } 0.5 < m < 1.0, \text{ and} \\ k_3 m^{-2.3} \text{ for } \geqslant 1.0. \end{cases}$$

For an MW IMF $\alpha_1 = 1.3$ and $\alpha_2 = 2.3$. The IMF above 1.0$M_\odot$ is assumed to have a Salpeter (1955) slope. The k_i's are normalization constants that ensure continuity of the IMF. The upper mass limit is 100 $M_\odot$ and the low-mass cutoff, m_c, is fixed at 0.08 $M_\odot$. In this Letter we present our IMF results in terms of $(M/L)_*$. The mass of the stellar population is calculated from the best-inferred slopes of the IMF, and stellar remnants are included in the final mass calculation following Conroy et al. (2009). A stellar population is considered bottom-heavy (an overabundance of low-mass stars) if the exponents on the first two terms are larger than the MW IMF and is considered bottom-light (a paucity of low-mass stars) if they are less than those values.

3.2. Mock Data Demonstrations

To test our ability to recover $(M/L)_*$ from the data, we synthesize mock spectra by assuming a Salpeter IMF, adding different amounts of noise, and then use our models and fitting procedures to derive $\Delta M/L_*$. We show $\Delta M/L_*$ for mock spectra with solar, $[Z/H] = 0.0$ (orange), and sub-solar, $[Z/H] = -1.0$ (blue) For each signal-to-noise ratio (S/N) and metallicity value we create 10 mock spectra with fixed S/N per Å over the wavelength range 0.4–1.015 μm, a velocity dispersion of 250 km s^{-1}, and an age of 10 Gyr. The abundance patterns of the mock spectra are solar scaled (e.g., Choi et al. 2016) and the nuisance parameters are set to zero. The points shown in Figure 1 are the median values of the differences between the input $(M/L)_*$ and the derived $(M/L)_*$ from the inferred IMF parameters for each metallicity and S/N pair. The uncertainties shown are the median statistical uncertainties of the recovered values.

For solar metallicity the models recover $(M/L)_*$ when the S/N $\gtrapprox$ 100 Å^{-1}. A similar trend is also seen in the low-metallicity mock data. While not a significant difference, it is somewhat counterintuitive that the $(M/L)_*$ at the low-S/N regime is better recovered for the low-metallicity mocks. It could be that in the low-S/N regime weaker metal lines help to distinguish IMF effects. Below S/N $\sim$ 100 Å^{-1} there will be large uncertainty and bias in the $(M/L)_*$ measurement. The

[5] Models fitted with only a single age and excluding the emission lines made a negligible effect on the inferred parameters for the GCs.

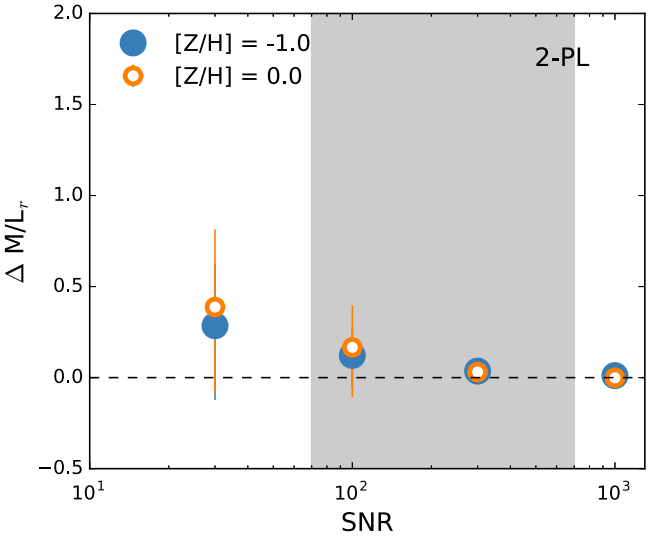

Figure 1. Recovery of $(M/L)_*$ from mock data as a function of S/N for $[Z/H] = 0.0$ (orange) and $[Z/H] = -1.0$ (blue) models. The circles show the median difference between the input $(M/L)_*$ and the inferred $(M/L)_*$ derived from the fits of 10 realizations of mock data. An S/N of $\gtrsim$100 is needed to recover the *M/L*. The gray band shows the range of S/N values in the data.

bias exists in the low-S/N regime because the priors become important and the truth is at the edge of the prior. The measurements are less sensitive to S/N if the true m_c is higher (see Conroy et al. 2017a for details). As discussed in Conroy et al. (2017a), the S/N requirements for allowing m_c to vary is even higher than what is shown in Figure 1. Most of the data in this Letter do not meet the S/N requirements for this type of parametrization.

4. Results

4.1. Basic Stellar Population Characteristics

In the upper panels of Figure 2 we compare the best-fit models (gray) and data for M31-B193 (orange), an MR GC, and M31-B058 (blue), an MP GC. In the lower panels we show the percentage difference between the models and the data. The uncertainty for M31-B058 is shown by the gray band (the uncertainty for M31-B193 is comparable). The CvD models would not have been able to fit M31-B058 because of the limited metallicity range, but with the C2V models the residuals between MP and MR GC are comparable and small.

In Table 1 we show the best-inferred median values for [Fe/H], mass-weighted age, [Mg/Fe], and the $(M/L)_*$ in Johnson *V* where we have and have not allowed the IMF to vary from Kroupa. Our stellar parameters are broadly consistent with previous work on these objects. From deep *Hubble Space Telescope* (*HST*)/Advanced Camera for Surveys (ACS) imaging of M32, Monachesi et al. (2012) inferred two dominant populations, one 2–5 Gyr and MR and an older population, ∼7 Gyr. Our inferred age skews young as the integrated light observations are almost certainly dominated by the young population. Monachesi et al. (2012) determined near-solar mass- and light-weighted metallicities for M32. Our inferred metallicity is slightly more MR than that. Janz et al. (2016) used Lick indices on M59-UCD3 and found $[Z/H] = 0.15 \pm 0.10$. Converting our value for [Fe/H] to [Z/H] (Trager et al. 2000) we get $[Z/H] \approx 0.2$, consistent with the Janz et al. (2016) value. Furthermore, our inferred values for M59-UCD3 are consistent with those presented in Sandoval et al. (2015) with a spectrum from a different instrument and an earlier iteration of our models.

Our inferred ages for M31-B163 and B193 are consistent with the ages derived by Colucci et al. (2014). This is particularly striking as Colucci et al. (2014) worked with high-resolution data and a completely different analysis technique. The age for M31-B058 is young for a GC but is consistent with previous work in modeling the integrated light of MP GCs (Graves & Schiavon 2008). In the case of M31-B058 there is a moderate blue horizontal branch that could be boosting the strength of the Balmer lines (Rich et al. 2005).

4.2. The IMF

For our main analysis we define the "IMF mismatch" parameter, $\alpha_{\rm IMF}$. This parameter is the ratio of $(M/L)_*$ where we have fitted for the IMF, to $(M/L)_*$ where we have assumed an MW IMF. In Figure 3 we show $\alpha_{\rm IMF}$ plotted against [Fe/H] (left), [Mg/Fe] (middle), and velocity dispersion (σ, right) for all of the objects in our sample: the M31 GCs (purple), M59-UCD3 (red), M32 (green). We supplement our data set with the ETG data from van Dokkum et al. (2017; gray open circle) with the same instrumental and model setups.

In Figure 4 we compare our $(M/L)_*$ measurements with available $(M/L)_{\rm dyn}$ measurements. In the left panel, we show the kernel density estimate (KDE) for [Fe/H] versus $(M/L)_{\rm dyn}$ for M31 GCs from Strader et al. (2011; contours, darker color indicates higher concentration of objects) along with our $(M/L)_*$ for three GCs. Published $(M/L)_{\rm dyn}$ measurements do not currently exist for M59-UCD3. However, in the middle panel we show the KDE of [Fe/H] versus $(M/L)_{\rm dyn}$ of the sample of UCDs from Mieske et al. (2013; we removed objects that belong to NGC 5128 owing to suspicions of spurious σ measurements) and $(M/L)_*$ for M59-UCD3. In the right panel of Figure 4 we compare $(M/L)_*$ for M32 with $(M/L)_{\rm dyn}$ from van den Bosch & de Zeeuw (2010), where the gray band represents the lower and upper limits given by the uncertainty. In each panel we show metallicity-dependent $(M/L)_*$ predictions using SSPs with MW IMFs and solar-scaled abundance patterns. The ages of the SSPs were chosen to approximate the inferred ages from full-spectrum fitting.

We note the slight discrepancy in Figures 3 and 4 in how much M32 appears to deviate from an MW IMF. This is due to the fact that the MW IMF in Figure 3 also accounts for non-solar abundance patterns, while the SSPs used to generate the orange lines in Figure 4 do not.

5. Discussion

McConnell et al. (2016) and Zieleniewski et al. (2017) computed line indices for a variety of ETGs and claimed that observed line strengths can be explained by abundance variations alone. These studies have driven debates about the extent IMF measurements are affected by the underlying abundance patterns. The M31 GCs are an excellent test bench for the models in this respect, as they have similar metallicities and element enhancements as massive ETGs. If the models did conflate metallicity and abundance effects with IMF effects we would expect to find similar $(M/L)_*$ enhancements in the M31 GCs. Recovering $\alpha_{\rm IMF} \sim 1$ for the M31 GCs over a wide metallicity range is a strong validation that our models can distinguish IMF and abundance effects.

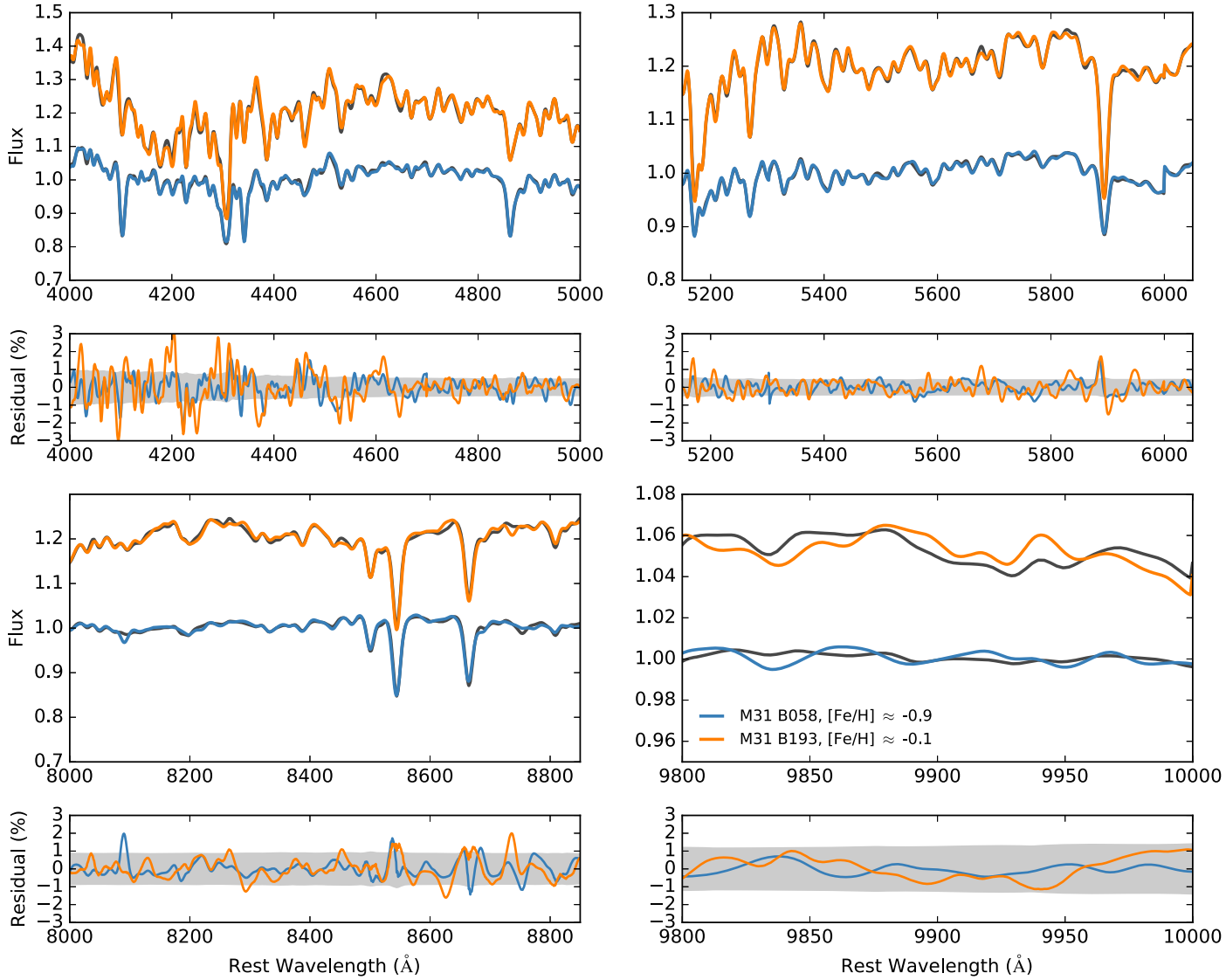

Figure 2. (Upper panels) Comparison of best-fit models (gray) and data in key wavelength regions for M31-B193 (MR GC; orange) and M31-B058 (MP GC; blue). (Lower panels) Comparison of the percentage difference between the best-fit model and data regions for M31-B193 and M31-B058. The data have been smoothed and so the pixels are highly correlated. In the gray band we show the uncertainty for one of the GCs, M31-B058, as the uncertainties are comparable. The residuals between MR and MP GC are also comparable.

Table 1
List of Objects and Associated Physical Parameters

Object	S/N Å^{-1}	σ (km s^{-1})	[Fe/H]	Age (Gyr)	[Mg/Fe]	M/L$_V$ 2 PL	M/L$_V$ MW
M32	730[aa]	75[a]	$0.15^{+0.01}_{-0.01}$	$2.98^{+0.05}_{-0.06}$	$0.02^{+0.04}_{-0.01}$	$2.4^{+0.64}_{-0.64}$	$1.63^{+0.03}_{-0.03}$
M59-UCD3	70	70[b]	$0.01^{+0.01}_{-0.01}$	$7.7^{+0.49}_{-0.48}$	$0.18^{+0.01}_{-0.01}$	$5.1^{+0.87}_{-1.17}$	$2.98^{+0.11}_{-0.1}$
M31-B163	100	21[c]	$-0.18^{+0.01}_{-0.01}$	$11.37^{+0.7}_{-0.61}$	$0.21^{+0.01}_{-0.01}$	$3.61^{+0.59}_{-0.49}$	$3.34^{+0.12}_{-0.11}$
M31-B193	250	19[c]	$-0.11^{+0.01}_{-0.01}$	$9.7^{+0.54}_{-0.45}$	$0.24^{+0.01}_{-0.01}$	$2.69^{+0.43}_{-0.2}$	$3.16^{+0.09}_{-0.1}$
M31-B058	120	23[c]	$-0.96^{+0.01}_{-0.01}$	$6.92^{+0.09}_{-0.1}$	$0.37^{+0.02}_{-0.02}$	$1.38^{+0.07}_{-0.08}$	$1.54^{+0.01}_{-0.01}$

Notes. Mean best-inferred value for each parameter is shown with 1σ statistical uncertainty. Values were determined with our models and fitting procedure, as described in Section 3.1. The penultimate column are the $(M/L)_*$ values where the IMF was allowed to vary as a two-component power-law IMF, and the last column is the $(M/L)_*$ values where the IMF was fixed to a Kroupa IMF.

[aa] Although the S/N is high it was cloudy at the time of observation so there is additional uncertainty in the data not represented by Poisson statistics.

[a] Gültekin et al. (2009).

[b] Janz et al. (2016).

[c] Strader et al. (2011).

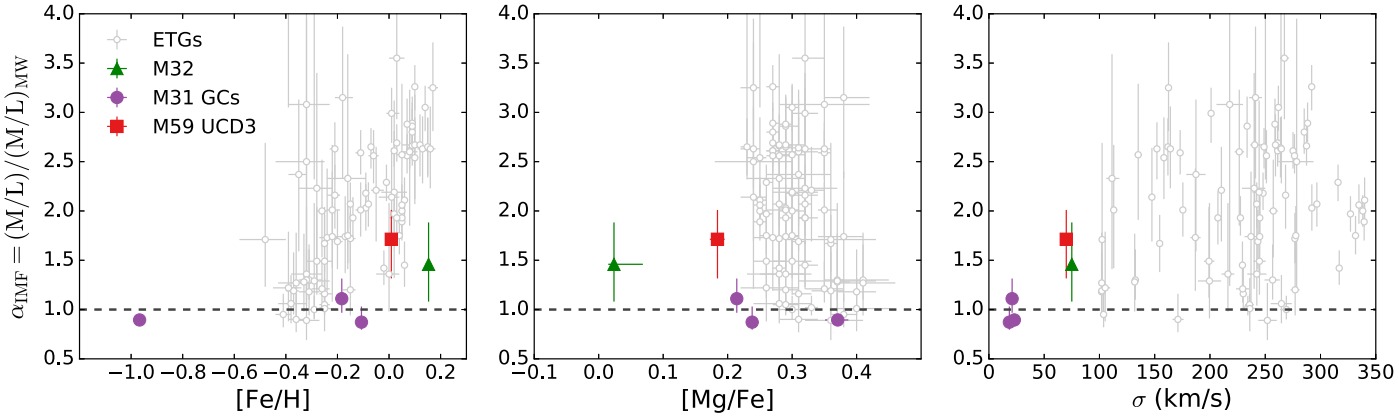

Figure 3. IMF mismatch parameter plotted against [Fe/H] (left), [Mg/Fe], (middle), and σ (right) for the two-component power-law IMF. Values shown are for M59-UCD3 (red squares), the M31 GCs (purple circles), and M32 (green triangles). We show the full sample of ETG local values from van Dokkum et al. (2017; open gray circles).

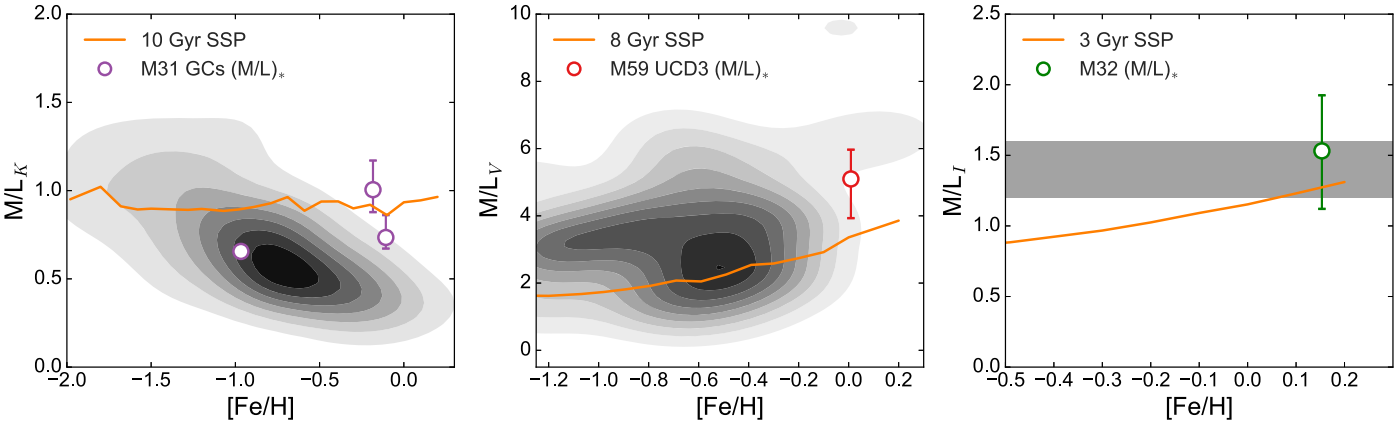

Figure 4. Comparison of $(M/L)_{\rm dyn}$ (gray) to $(M/L)_*$ values for M31 GCs (left; purple), M59-UCD3 (middle; red), and M32 (right; green). In each panel we show the metallicity-dependent $(M/L)_*$ predicted from SSPs with Kroupa IMF and solar-scaled abundance patterns. The ages of the SSPs (orange line) were chosen to approximate the inferred ages from our full-spectrum fitting. Our inferred $(M/L)_*$ values for M59-UCD3 and M32 are consistent with available $(M/L)_{\rm dyn}$ measurements. There remain inconsistencies between the dynamical and stellar measurements at high metallicity for the M31 GCs.

Our modeling of the M31 GCs improves upon earlier work in several important ways. Zonoozi et al. (2016) did not fit models to data and assumed a top-heavy IMF. Conroy & van Dokkum (2012) used a stacked spectrum of MR GCs to test the CvD models while making measurements for individual clusters and included a MP GC. The lack of expected dark matter in GCs means that dynamical measurements provide tight constraints on our expectations for $(M/L)_*$. This makes the continued discrepancy between dynamical and stellar measurements on the MR end of the M31 GCs troubling.

For the current models m_c is fixed at 0.08 $M_\odot$, but a higher m_c would lower the inferred $(M/L)_*$ values. Chabrier et al. (2014) explored the different theoretical conditions that would create a higher m_c, while there is empirical evidence that the IMF in GCs becomes flatter for $<0.5M_\odot$ (Marks et al. 2012), which would mimic an increase in m_c. It is not out of the realm of possibility that m_c could differ from our fiducial value. However, it takes increasing m_c to $0.5M_\odot$, an extreme value, to decrease $(M/L)_*$ by 35%, i.e., closer to the locus of the MR $(M/L)_{\rm dyn}$ values. It is premature to make any definitive conclusions, but these preliminary results suggest that a variable IMF cannot explain the [Fe/H] versus $(M/L)_{\rm dyn}$ trend for the M31 GCs. Zonoozi et al. (2016) were able to achieve better agreement by making ad hoc adjustments to the retention rates of stellar remnants in the GCs. Follow-up work with a larger sample and more detailed physical models is required.

The mild bottom-heaviness of M59-UCD3 contrasts with the expectations of Dabringhausen et al. (2012) and Marks et al. (2012). That is not to say that our results are in direct contradiction with either study. First, those studies are tracing the high-mass stars, and we are tracing the low-mass stars. Second, it is becoming increasingly clear that, as a class, UCDs encompass a diverse set of objects (Janz et al. 2016). Until we have a better understanding of a more comprehensive sample of objects, it is premature to make any firm conclusions about how UCDs *as a whole* behave.

For the sample presented in this work, the main feature of Figure 3 is that the CSSs are distinct from the main ETG sample. Though they span large [Fe/H] and [Mg/Fe] ranges, they vary much less in $\alpha_{\rm IMF}$ than the ETG sample. Both M59-UCD3 and M32 have elevated $\alpha_{\rm IMF}$ values but are not on the main [Fe/H]–$\alpha_{\rm IMF}$ trend for massive ETGs. M59-UCD3 is in a cluster of ETG points that also deviate from the main trend. Those points originate from the central regions of just two of the galaxies in the ETG sample: NGC 1600 and NGC 2695.

The main conclusion of this work is that metallicity is not the sole driver of IMF variability (see Martín-Navarro et al. 2015; van Dokkum et al. 2017). The right panel of Figure 3 suggests that velocity dispersion is also associated with IMF variation.

This is an important result because different theoretical frameworks will be controlled by different fundamental variables, depending on the kind of physics they evoke to fragment gas clouds (see Krumholz 2014). By expanding IMF probes into the parameter space that CSSs occupy, we can elucidate what these variables are.

Moreover, it is unclear how theoretical frameworks of star formation should treat monolithically formed populations (GCs, some UCDs) as compared with populations that build up over time (some CSSs and ETGs; see Ch. 13 in Kroupa et al. 2013). By measuring the IMFs of CSSs with the same modeling framework that we do for ETGs, we can obtain a self-consistent observational picture of how the IMF manifests in the different types of population. Currently, with our small sample, it is unclear whether the GCs have IMFs that are distinct from the UCDs and cEs (the left and middle panels of Figure 3), or are a part of the same continuum (right panel of Figure 3).

The authors wish to recognize and acknowledge the very significant cultural role and reverence that the summit of Mauna Kea has always had within the indigenous Hawaiian community. A.V. is supported in part by an NSF Graduate Research Fellowship. J.B. acknowledges support from NSF grants AST-1518294 and AST-1616598. C.C. acknowledges support from NASA grant NNX15AK14G, NSF grant AST-1313280, and the Packard Foundation. A.J.R. was supported by NSF grants AST-1515084 and PHY11-25915, and as a Research Corporation for Science Advancement Cottrell Scholar. The authors would like to thank A. Seth, C. Ahn, J. Strader, and I. Martín-Navarro for helpful discussion and the anonymous referee, whose thoughtful comments improved the quality of this manuscript.

Software: `astropy` (Astropy Collaboration et al. 2013), `matplotlib` (Hunter 2007), `NumPy` (Van Der Walt et al. 2011), `Seaborn` (Waskom et al. 2014).

ORCID iDs

Alexa Villaume https://orcid.org/0000-0003-1887-0621
Jean Brodie https://orcid.org/0000-0002-9658-8763
Charlie Conroy https://orcid.org/0000-0002-1590-8551
Aaron J. Romanowsky https://orcid.org/0000-0003-2473-0369
Pieter van Dokkum https://orcid.org/0000-0002-8282-9888

References

Astropy Collaboration, Robitaille, T. P., Tollerud, E. J., et al. 2013, A&A, 558, A33
Cappellari, M., Scott, N., Alatalo, K., et al. 2013, MNRAS, 432, 1709
Cenarro, A. J., Gorgas, J., Vazdekis, A., Cardiel, N., & Peletier, R. F. 2003, MNRAS, 339, L12
Chabrier, G., Hennebelle, P., & Charlot, S. 2014, ApJ, 796, 75
Choi, J., Dotter, A., Conroy, C., et al. 2016, ApJ, 823, 102
Cohen, J. G. 1978, ApJ, 221, 788
Colucci, J. E., Bernstein, R. A., & Cohen, J. G. 2014, ApJ, 797, 116
Conroy, C., Gunn, J. E., & White, M. 2009, ApJ, 699, 486
Conroy, C., & van Dokkum, P. G. 2012, ApJ, 760, 71
Conroy, C., van Dokkum, P. G., & Villaume, A. 2017a, ApJ, 837, 166
Conroy, C., Villaume, A., van Dokkum, P., & Lind, K. 2017b, ApJ, submitted
Dabringhausen, J., Kroupa, P., Pflamm-Altenburg, J., & Mieske, S. 2012, ApJ, 747, 72
Faber, S. M., & French, H. B. 1980, ApJ, 235, 405
Ferreras, I., La Barbera, F., de la Rosa, I. G., et al. 2013, MNRAS, 429, L15
Foreman-Mackey, D., Hogg, D. W., Lang, D., & Goodman, J. 2013, PASP, 125, 306
Goodman, J., & Weare, J. 2010, Commun. Appl. Math. Comput. Sci., 5
Graves, G. J., & Schiavon, R. P. 2008, ApJS, 177, 446
Gültekin, K., Richstone, D. O., Gebhardt, K., et al. 2009, ApJ, 698, 198
Hunter, J. D. 2007, CSE, 9, 90
Janz, J., Norris, M. A., Forbes, D. A., et al. 2016, MNRAS, 456, 617
Jerabkova, T., Kroupa, P., Dabringhausen, J., Hilker, M., & Bekki, K. 2017, A&A, in press (arXiv:1708.07127)
Kroupa, P., & Gilmore, G. F. 1994, MNRAS, 269
Kroupa, P. 2001, MNRAS, 322, 231
Kroupa, P., Weidner, C., Pflamm-Altenburg, J., et al. 2013, in Planets, Stars and Stellar Systems. Volume 5: Galactic Structure and Stellar Populations, ed. T. D. Oswalt & G. Gilmore (Dordrecht: Springer), 115
Krumholz, M. R. 2014, PhR, 539, 49
La Barbera, F., Ferreras, I., Vazdekis, A., et al. 2013, MNRAS, 433, 3017
Lyubenova, M., Martín-Navarro, I., van de Ven, G., et al. 2016, MNRAS, 463, 3220
Marks, M., Kroupa, P., Dabringhausen, J., & Pawlowski, M. S. 2012, MNRAS, 422, 2246
Martín-Navarro, I., Vazdekis, A., La Barbera, F., et al. (The CALIFA Team) 2015, ApJL, 806, L31
Martín-Navarro, I. MNRAS, 456, L104
McConnell, N. J., Lu, J. R., & Mann, A. W. 2016, ApJ, 821, 39
Mieske, S., Frank, M. J., Baumgardt, H., et al. 2013, A&A, 558, A14
Monachesi, A., Trager, S. C., Lauer, T. R., et al. 2012, ApJ, 745, 97
Newman, A. B., Smith, R. J., Conroy, C., Villaume, A., & van Dokkum, P. 2016, ApJ, submitted
Oke, J. B., Cohen, J. G., Carr, M., et al. PASP, 107, 375
Pandya, V., Mulchaey, J., & Greene, J. E. 2016, ApJ, 162, 162
Portegies, S. F., McMillan, S. L. W., & Gieles, M. 2010, ARA&A, 48, 431
Rich, R. M., Corsi, C. E., Cacciari, C., et al. 2005, AJ, 129, 2670
Salpeter, E. E. 1955, ApJ, 121, 161
Sandoval, M. A., Vo, R. P., Romanowsky, A. J., et al. 2015, ApJL, 808, L32
Smith, R. J. 2014, MNRAS, 443, L69
Spiniello, C., Koopmans, L. V. E., Trager, S. C., Czoske, O., & Treu, T. 2011, MNRAS, 417, 3000
Strader, J., Caldwell, N., & Seth, A. C. 2011, AJ, 142, 8
Trager, S. C., Faber, S. M., Worthey, G., & González, J. J. 2000, AJ, 119, 1645
Treu, T., Auger, M. W., Koopmans, L. V. E., et al. 2010, ApJ, 709, 1195
van den Bosch, R. C. E., & de Zeeuw, P. T. 2010, MNRAS, 401, 1770
Van Der Walt, S., Colbert, S. C., & Varoquaux, G. 2011, arXiv:1102.1523
van Dokkum, P., Conroy, C., Villaume, A., Brodie, J., & Romanowsky, A. J. 2017, ApJ, 841, 68
van Dokkum, P. G., & Conroy, C. 2010, Natur, 468, 940
Villaume, A., Conroy, C., Johnson, B., et al. 2017, ApJS, 230, 23
Waskom, M., Botvinnik, O., O'Kane, D., et al. 2014, mwaskom/seaborn: v0.8.0 (July 2017), Zenodo, doi:10.5281/zenodo.824567
Wing, R. F., & Ford, W. K., Jr. 1969, PASP, 81, 527
Zieleniewski, S., Houghton, R. C. W., Thatte, N., Davies, R. L., & Vaughan, S. P. 2017, MNRAS, 465, 192
Zonoozi, A. H., Haghi, H., & Kroupa, P. 2016, ApJ, 826, 89